

Impact of ligand-mediated inductive effects on electrochemical p-doping of CsPbBr₃ nanocrystals

Theresa Hettiger, Roshini Jayabalan, Arup Sarkar, Jonas L. Hiller, Max Nusshör, Denis Andrienko, Wolfgang Brütting, Marcus Scheele

Angaben zur Veröffentlichung / Publication details:

Hettiger, Theresa, Roshini Jayabalan, Arup Sarkar, Jonas L. Hiller, Max Nusshör, Denis Andrienko, Wolfgang Brütting, and Marcus Scheele. 2026. "Impact of ligand-mediated inductive effects on electrochemical p-doping of CsPbBr₃ nanocrystals." ACS Energy Letters 11 (1): 567-72.
<https://doi.org/10.1021/acsenenergylett.5c03184>.

Impact of Ligand-Mediated Inductive Effects on Electrochemical p-Doping of CsPbBr₃ Nanocrystals

Theresa Hettiger, Roshini Jayabalan, Arup Sarkar, Jonas L. Hiller, Max Nusshör, Denis Andrienko, Wolfgang Brütting, and Marcus Scheele*




Cite This: *ACS Energy Lett.* 2026, 11, 567–572



Read Online

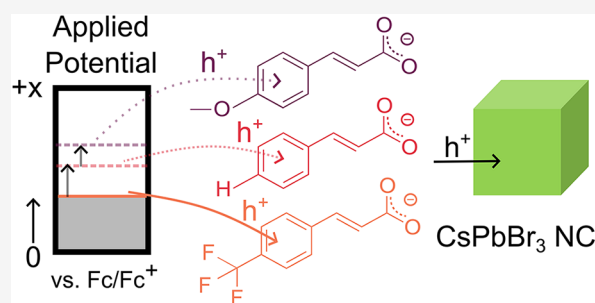
ACCESS |

 Metrics & More

 Article Recommendations

 Supporting Information

ABSTRACT: Lead halide perovskite nanocrystals (NCs) are promising materials for light-emitting diodes (LEDs) due to their wavelength tunability, narrow emission line width, and high photoluminescence quantum yield. Oftentimes, these devices suffer from charge carrier imbalance and reduced charge injection because as-synthesized NCs are covered by long aliphatic ligands. Here, we report ligand exchange to small electron-withdrawing or -donating cinnamate ligands. We probe the influences of the ligands' inductive effect on hole injection by photoluminescence spectroelectrochemistry (PL SEC). We find that hole injection into NCs covered by electron-withdrawing ligands is facilitated, and hole-only devices exhibit higher currents compared to electron donating ligands. Our work highlights the potential of PL SEC as a powerful tool to rationalize the performance of lead halide perovskite NCs in LEDs.



Lead halide perovskites have attracted the attention of many researchers due to a small exciton binding energy, emission wavelength tunability, and a trap-free band gap.^{1,2} All these properties make them interesting for the application in LEDs or solar cells.^{3–8} For both devices, efficient and balanced charge injection/extraction is essential. This requires that the absolute energy level of the perovskite layer is well-aligned with those of the hole and electron transport layers, enabling efficient energy transfer and ensuring that charge carriers can be injected/extracted effectively.⁹ Both problems can be addressed by small organic molecules.¹⁰ For instance, in solar cells, electrode surfaces are modified by organic molecules to improve charge extraction.^{11–14}

When considering LEDs, perovskite NCs are used because of their high photoluminescence quantum yield, easy tunability through halide exchange, and narrow emission profile.^{2,15–18} These NCs are covered by an organic ligand shell that provides the possibility of tuning charge injection and their optoelectronic properties.^{19–21} In solution, the same ligand shell is crucial for the colloidal stability of the NCs.²² In comparison to other NCs, the organic ligand shell of CsPbX₃ (X = Cl, Br, I) NCs is described by a dynamic ligand binding model.^{23,24} Here, de Roo et al. have reported, following the synthesis according to Protesescu et al., that oleylamine (OAm) binds to the surface, while oleic acid (OA) binds only when OAm is present in excess.²³ Chen et al. have presented another model

with OA binding to Cs⁺ on the surface.²⁵ Given the low stability and the inconsistent picture of the surface ligands, researchers try to modify these NCs to increase their stability either by introducing zwitterionic ligands like lecithin or using didodecyltrimethylammonium bromide (DDABr) and other amine containing ligands.^{26–28} Both of these systems still lack one characteristic that is essential for building devices: Due to the presence of aliphatic ligand chains, injecting holes or electrons into NCs covered by these ligands becomes more challenging. This can only be achieved by ligand stripping or using π -conjugated ligands.^{19,29–31}

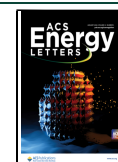
In this context, cinnamic acid (CA) derivatives provide an opportunity to study the influence of electron withdrawing and electron donating groups on the charge injection into perovskite NCs, similar to work performed on PbS NCs.³² Via substitution at the phenyl ring, these functional groups can exert large inductive effects on the NC via a short π -conjugated

Received: October 3, 2025

Revised: December 13, 2025

Accepted: December 15, 2025

Published: December 23, 2025



system. An additional advantage of these molecules is their cost-effectiveness and widespread availability.

Testing charge injection by probing the absolute energy levels can be done by performing ultrahigh vacuum methods like X-ray and UV photoelectron spectroscopy (XPS, UPS).³³ This probes the energy levels of the NC directly. Using this method, Kroupa et al. determined that the valence band (VB) of PbS NCs with electron withdrawing ligands on their surface shifts to higher energies, resulting in a hindered hole injection, while hole injection into NCs covered by electron donating ligands is facilitated.³² Lu et al. probed charge transfer on cinnamate and 3,5-difluorocinnamate-covered CsPbBr₃ NCs indirectly by determining their photoredox activity. Their results showed easier electron extraction due to the attached π -conjugated system.³⁴ However, precise values in how strongly electron extraction can differ between these attached ligands to the NCs are still missing.

Another way of probing charge injection is spectroelectrochemistry (SEC). Here, an electrochemical method, e.g., cyclic voltammetry (CV), is combined with a spectroscopic technique, like PL or absorbance measurements.^{35–37} By this method, the NCs with their organic ligand shell are drop-cast or spin-coated on a transparent working electrode, which allows for simultaneous charge injection and optical measurements. This makes the measurements sensitive to influences by the surface ligands on charge injection. Mulder et al. were already able to electrochemically p-dope CsPbBr₃ NCs at 0.9 V vs NHE.³⁸ Using this method to probe perovskite NCs is challenging, since they are prone to decomposition. Additionally, the electrochemical window is limited by Pb²⁺ reduction and oxidation and Br⁻ oxidation.^{38,39} Still, staying within a moderate electrochemical window and looking at the emission simultaneously make SEC a powerful method to study charge injection.

In this work, we demonstrate a successful ligand exchange of oleate-covered CsPbBr₃ NCs to 4-trifluoromethylcinnamate (CACF₃) as an electron withdrawing ligand, and cinnamate (CAH), methoxycinnamate (CAOMe), 4-dimethylaminocinnamate (CAN(Me)₂) as electron donating ligands. We study these modified NCs using SEC PL on a confocal optical setup and determine the necessary potential for hole injection, depending on the functionality of the ligand. Our results show that charge injection can be tuned by 0.31 eV. The facilitated hole injection behavior of CACF₃-covered NCs is supported by their performance in LEDs and in hole-only devices.

We synthesize oleate-covered CsPbBr₃ NCs following the method of Yassitepe et al.⁴⁰ By using tetraoctylammonium bromide, the ligand sphere of the NCs consists exclusively of carboxylates, which we find beneficial for ligand exchange. These NCs are cubic with an average size of 8.9 nm and show absorption at 505 nm and a PL peak at 510 nm. We exchange the oleate ligands with cinnamic acid derivatives using precipitation and resuspension method. Additionally, we remove OA from the surface of the NCs by precipitating the particles with hexane as antisolvent. Figure 1 shows a scheme of the ligand exchange process with the different CAs, each distinguishable by their color code, along with an exemplary characterization of the NCs after exchanging the ligand with CACF₃ as the surface molecule. We find a peak PL at 509 nm, and an average size of 8.7 nm, which is within its standard deviation before the ligand exchange.

We provide full exchange protocols and characterization of the exchanged NCs in the Supporting Information (SI) –

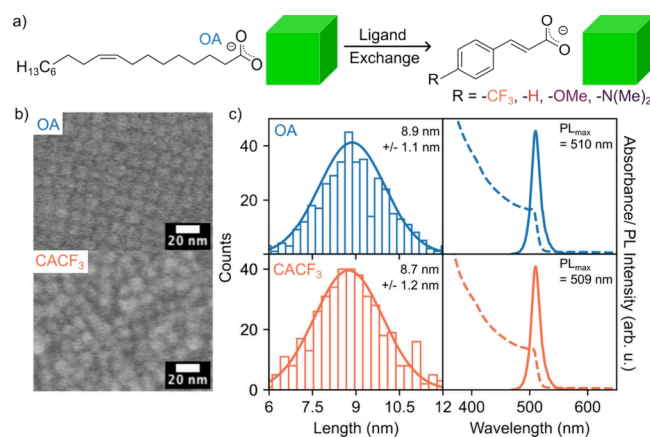


Figure 1. a) Scheme of surface ligand exchange of OA-covered CsPbBr₃ NCs to R-CA-covered NCs with R = CF₃, H, OMe, and N(Me)₂. b) SEM images of OA-covered NCs (top) and CACF₃-covered NCs (bottom). c) Extracted sizes fitted to normal distribution (on the left), PL (solid lines), and absorbance spectra (dashed lines) of OA-covered NCs (top) and CACF₃-covered NCs (bottom) on the right.

Materials and Methods, as well as in Figures S1–S3. To monitor the success of ligand exchange, we employ ¹H NMR spectroscopy in SI – Figure S4.

We investigated charge injection into R-CA-covered NCs with SEC PL according to the simplified schematic in Figure 2a. Briefly, we excite the NCs at 405 nm (blue arrow) and

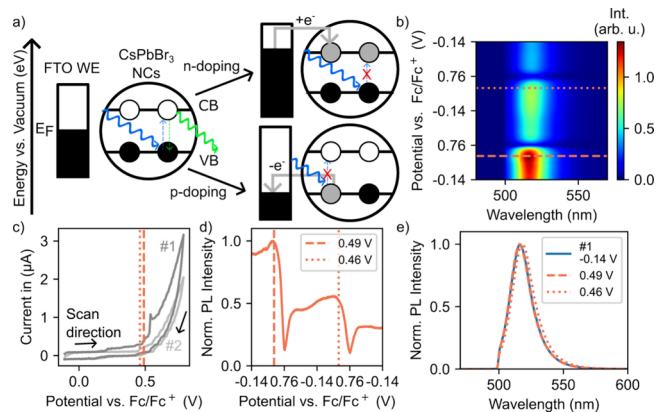


Figure 2. a) Schematic illustration of electrochemical p- and n-doping of the electronic structure of the NC with its conduction (CB) and valence band (VB) and the resulting dark state of the NC. b) PL spectra of CACF₃-covered NCs with a scan speed of 2 mV/s with a marked switching potential at 0.76 V and marked onset potential of VB (dashed, orange). c) Two consecutive CV scans in the oxidative direction during SEC PL with marked onset potential determined by PL intensity decay from d). d) Maximum PL intensity trace of CACF₃ NC emission extracted from panel b (solid, orange). e) Extracted single spectra at the beginning of the measurement (blue, -0.14 V) and onset potentials of charge injection (dashed, orange).

monitor the variation in PL intensity (green arrow) under varying electrochemical potential. While applicable to oxidation and reduction alike, we limit ourselves here to the oxidative direction and the effect of electrochemical p-doping. To this end, we lower the potential of the working electrode (WE, E_F) starting from the open circuit potential (E_{OC}) toward the valence band (VB) of the NC (right-hand side, Figure 2a).

As E_F approaches the VB, electrons are extracted from the NC, leading to vacancies in the VB, that is, p-doping. This reduces the rate of absorption (red cross, right-hand side; Figure 2a) and, consequently, the PL intensity. The success of p-doping and the required electrochemical potential can therefore be inferred from the potential-dependent PL scans.

We note that all R-CA-covered NC samples exhibit some degree of photobleaching caused by the exposure to the electrolyte solution ($\text{CH}_3\text{CN}/\text{TBAHFP}$) and/or laser radiation without applying any potential as detailed in the SI – Figure S7. This is expected due to the poor tolerance of lead halide perovskites to polar solvents. By convention, we reference all SEC data against the half-wave potential of the ferrocene/ferrocenium redox couple (Fc/Fc^+) in the same electrochemical cell and electrolyte solution (SI – Figure S8, spectroelectrochemistry cell in SI – Figure S9).

We display the results of an exemplifying SEC PL spectral series for CACF_3 -covered NCs in Figure 2b with a 2 mV/s sweep rate and 1 s spectral integration time. The recorded cyclic voltammogram during this measurement is depicted in Figure 2c. A spectral slice of the series in Figure 2b taken at the PL maximum reveals abrupt darkening at 0.49 V (Figure 2d), which we attribute to the beginning of the hole injection. To prevent oxidative decomposition, we switch the scan direction at 0.76 V toward the open circuit potential at -0.14 V, after which we initiate the next scan cycle. The mostly identical shape compared to the first cycle, including a comparable potential for hole injection (0.46 V), indicates a large degree of reversibility of this action. This is supported by the spectral shape of the three PL measurements taken at the open circuit potential and the onset potentials of charge injection, which are overlaid in Figure 2e to showcase their almost identical shape and spectral position.

We continue with an analogous SEC PL analysis of CAH- and CAOMe-covered NCs in Figure 3. Both samples exhibit

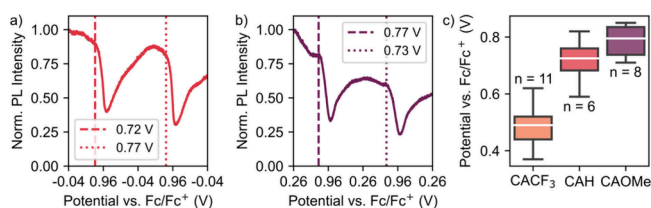


Figure 3. Normalized PL intensity trace as a function of the applied potential for a) CAH-covered NC. b) CAOMe-covered NCs. c) Summary of onset potentials for hole injection of different CA-R-covered NCs with number of measurements n and medians of hole injection onset potentials (in white) at 0.49 V (CACF_3), 0.73 V (CAH), and 0.8 V (CAOMe) vs Fc/Fc^+ .

qualitatively similar behavior to the previously discussed scan for CACF_3 -covered NCs in Figure 2d, however at significantly more oxidative potentials (0.72–0.77 V). Figure 3c provides a summary of the statistical average ($n = 6$ to 11) of all three hole injection potentials with 0.49 V for CACF_3 -covered NCs, 0.73 V for CAH- and 0.8 V for CAOMe-coverage. For device purposes, we note that these values correspond approximately to -5.39 eV, -5.63 eV, and -5.7 eV on the electronic energy scale vs vacuum for CACF_3 -, CAH- and CAOMe-coverage, respectively, taking the Fc/Fc^+ half-wave potential at -4.9 eV vs. vacuum as a widely accepted reference point.⁴¹

We did not succeed with reversible hole injection into CANMe_2 -covered NCs (see SEC PL data in the SI – Figure

S13a). Our CV data of pure CANMe_2 suggest that the ligand itself decomposes irreversibly before holes are injected into the NCs (see SI – Figure S13b).

We investigate the performance in LEDs in Figure 4 of the three R-CA-covered NC systems that exhibit a reversible hole

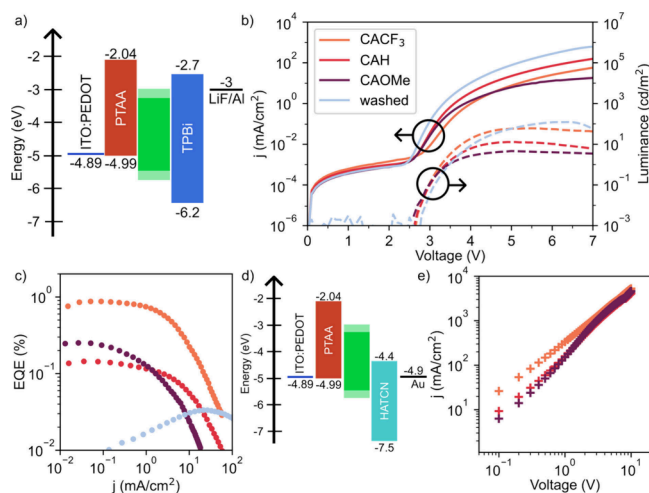


Figure 4. Characterization of CA-R/OAM and ligand-stripped NC (washed, light blue) LEDs. a) Flat-band energy diagram of LED with CsPbBr_3 NCs as emissive layer (green). b) Current density (j , solid lines) and luminance (dashed lines) vs voltage. c) EQE vs j . d) Flat-band energy diagram of hole-only device. e) j vs voltage from single carrier devices (holes).

injection. Since exceptionally high colloidal stability is crucial for device fabrication, we had to modify the NC ligand exchange procedure according to Protesescu et al.¹⁵ Briefly, we first precipitated the as-synthesized NCs and exposed them to a mixture of OAM (which increases colloidal stability) and one of the three R-CA derivatives. For each CA, the ratio of ligands was kept the same, with the goal of addressing differences in the LED behavior relative to the introduced CAs. In addition, NCs after two precipitation/washing steps without adding new ligands (washed) are investigated as a reference.

Figure 4a shows the energy level diagram of the built devices. Energy levels for the transport layers were sourced from previously published reports.^{30,42,43} In the case of the cinnamate-covered NCs, we extracted the valence band position from the hole-injection potential measured by SEC PL (-5.37 to -5.71 eV), while we obtained the conduction band position by adding the optical band gap determined from PL measurements. Figure 4b presents the current density–voltage–luminance (j – V – L) characteristics of the fabricated LEDs including the ligand stripped (washed, light blue) LEDs.

In the case of ligand stripping, we observe V_{on} at ~ 2.4 V and a luminance onset at ~ 2.8 V with a maximum luminance of ~ 120 cd/m². While the facilitated charge injection compared to as-synthesized NCs (SI – Figure S21) may appear substantial, the EQE– j characteristics (Figure 4c) reveal a steady increase in EQE with rising current density, with a peak value of 0.033% at ~ 20 mA/cm², characteristic of trap-filling behavior, followed by a sharp roll-off. This is consistent with a more exposed NC surface after ligand removal. Moreover, the electroluminescence (EL) spectrum of these ligand-stripped devices (SI – Figure S22) displays a broad parasitic emission at ~ 420 nm, attributed to the PTAA hole transport layer

(HTL),³⁰ indicating electron leakage through the emissive layer and subsequent recombination in the HTL.

In contrast, devices passivated with cinnamate ligands display lower current densities compared with the ligand-stripped NCs, but with comparable V_{on} (~ 2.4 V) and a slightly earlier luminance onset (~ 2.6 V). Among the cinnamates, CAOMe (purple) yields the lowest current density and reduced luminance output, indicating impeded carrier injection. We detected the highest luminance for CACF₃-covered NCs (orange), which can also be observed in their EQE- j characteristics (Figure 4c): CACF₃ exhibits more stable EQE values at low current densities ($\sim 0.8\%$) compared to CAH and CAOMe, suggesting improved carrier balance enabled by enhanced hole injection. EL spectra (SI – Figure S22) at 0.1 and 1 mA further confirm the trend that CACF₃ devices show stable emission exclusively from the NCs, whereas CAH and CAOMe devices exhibit additional parasitic emission from HTL. Despite these improvements, all cinnamate-based devices exhibit notable EQE roll-off at higher current densities, underscoring the limited stability of these NCs.

Additionally, we prepared hole-only devices (flat-band energy diagram⁴⁴ in Figure 4d) to study single carrier injection that might indicate some correlation to the SEC PL measurements on hole injection directly into the NCs. Figure 4e shows the highest current for CACF₃ covered NCs followed by that for CAH and CAOMe. This result indicates that holes are more easily transferred to the NCs covered by CACF₃ than the electron donating ligands on the NC surface present in LEDs.

We investigated the influence of π -conjugated cinnamate ligands with varying electron-donating and electron-withdrawing substituents on charge injection into CsPbBr₃ NCs. A general trend emerges: NCs functionalized with electron-withdrawing ligands exhibit hole injection at applied potentials lower than those of their electron-donating counterparts (Figure 3c). This view is supported by the hole-only devices in Figure 4e where the electron-withdrawing ligand CACF₃ invokes the largest current densities. We note that these results are counterintuitive considering previous XPS studies on PbS NCs.³² In those systems, the attachment of electron-withdrawing cinnamates shifted the absolute band edge positions toward higher potentials, thereby making hole injection more difficult. This discrepancy motivated us to compute the electronic structure near the band gap of CsPbBr₃ NCs covered with the three cinnamates applied here using PBE-D3 DFT functional (see Computational details in the Supporting Information). As expected, the highest molecular orbital (HOMO) energies of the pure R-CA molecules follow the order $-\text{CF}_3 < -\text{H} < -\text{OMe}$, highlighting that CACF₃ has the highest ionization potential (SI – Figure S23). When these molecules are attached to the NC surface, the valence band edge positions of the NCs follow the same qualitative trend; that is, the potential for hole injection into CACF₃-covered NCs is the highest (SI – Figure S23). We varied the binding sites and the number of molecules attached to the NC surface to find that the differences in hole injection potential decrease and converge toward the value calculated for bare NCs upon using fewer ligands (SI – Figure S24). These computational results indicate that R-CA binding should have a significant effect on the hole injection potential of CsPbBr₃ NCs, and the effect is qualitatively comparable to the aforementioned studies with PbS NCs.³² However, they are in contradiction to our

SEC PL and LED results, suggesting that a kinetic, rather than thermodynamic, factor is important for hole injection into CsPbBr₃ NCs.

A likely source for kinetic hindrance of charge carrier injection into the as-synthesized perovskite NCs are the long-chain aliphatic ligands OA and OAm, which are electrically insulating. Both, LED (SI – Figure S21) and SEC PL measurements confirm negligible charge transfer for this system, and cyclic voltammograms display only capacitive currents (SI – Figure S25). Ligand stripping removes these insulating chains, exposing under-coordinated surface sites that facilitate direct charge injection into the NCs with notable effects on the LED performance (Figure 4b,c) and PL quenching in SEC experiments (SI – Figure S26). A disadvantage is the large number of traps formed by this action, for which we find evidence in the EQE determination (Figure 4c) that requires large current densities to become significant, presumably because traps need to be filled first.

A good compromise between the two extremes of a dense, insulating ligand sphere vs no ligands at all are the cinnamate ligands employed in this study. Their π -systems provide an efficient electronic bridge between the NC and the electrode. We hypothesize that in the most electron-withdrawing ligand CACF₃, electron density is shifted from the NC core toward the ligand, leading to stabilization of the VB electrons through delocalization into the ligand π -system. In such a scenario, the VB of the NC and the HOMO of the ligand form a coupled electronic manifold. Hole injection into this shared state during SEC PL would therefore simultaneously deplete electron density from both NC and ligand, leading to a greatly reduced kinetic hindrance of hole injection. For the electron-richer cinnamates, the delocalization of the electron density from the NCs into the π -system is expected to be weaker.

Because SEC PL probes the coupled NC–ligand system as a whole, the trends observed in electrochemical measurements directly translate to LED operation: electron-withdrawing ligands facilitate hole injection and preserve emission intensity under high current densities, whereas electron-donating ligands exhibit reduced stability and higher injection barriers. This strong correlation between SEC PL and device data underscores the utility of SEC PL as a predictive tool for evaluating the interfacial charge-transfer properties in NC–ligand systems.

In this work, we have demonstrated successful ligand exchange strategies for cinnamic acid derivatives on CsPbBr₃ NCs. In addition, we have investigated charge injection into these NCs by SEC PL, focusing on hole injection. By using this method, we could derive an unexpected trend: hole injection into NCs with electron-withdrawing ligands attached is facilitated compared to electron-donating ligands. These findings are supported by the performance of the NCs in LEDs and hole-only devices. We address this behavior to different degrees of kinetic hindrance of charge carrier injection into the NCs through their ligand shell.

These findings emphasize the advantages of attaching directly π -conjugated ligands to NCs since they can influence the electronic properties and guarantee charge injection even at low bias. It also highlights the comparison of SEC PL and the performance in LEDs.

■ ASSOCIATED CONTENT

SI Supporting Information

The Supporting Information is available free of charge at <https://pubs.acs.org/doi/10.1021/acseenergylett.5c03184>.

Characterization of exchanged NCs; ^1H NMR spectra; stability of NCs in electrolyte solution; Fc/Fc^+ reference measurement; setup SEC cell; statistics on SEC PL; SEC PL on $\text{CAN}(\text{Me})_2$ covered NCs; CV of CA-Rs; characterization of CA-R/OAm NCs; SEM cross sections of LEDs; time-resolved PL; device performance; EL spectra; PBE-D3 computed molecular orbitals of CA-Rs attached to NCs; SEC PL on OA/OAm and OA covered NCs (PDF)

■ AUTHOR INFORMATION

Corresponding Author

Marcus Scheele – Institute for Physical and Theoretical Chemistry, University of Tübingen, 72076 Tübingen, Germany; orcid.org/0000-0002-2704-3591; Email: marcus.scheele@uni-tuebingen.de

Authors

Theresa Hettiger – Institute for Physical and Theoretical Chemistry, University of Tübingen, 72076 Tübingen, Germany

Roshini Jayabalan – Institute of Physics, University of Augsburg, 86135 Augsburg, Germany

Arup Sarkar – Max Planck Institute for Polymer Research, 55128 Mainz, Germany

Jonas L. Hiller – Institute for Physical and Theoretical Chemistry, University of Tübingen, 72076 Tübingen, Germany; orcid.org/0000-0002-4604-5816

Max Nuss Hör – Institute for Physical and Theoretical Chemistry, University of Tübingen, 72076 Tübingen, Germany

Denis Andrienko – Max Planck Institute for Polymer Research, 55128 Mainz, Germany; orcid.org/0000-0002-1541-1377

Wolfgang Brütting – Institute of Physics, University of Augsburg, 86135 Augsburg, Germany; orcid.org/0000-0001-9895-8281

Complete contact information is available at:

<https://pubs.acs.org/doi/10.1021/acseenergylett.5c03184>

Notes

The authors declare no competing financial interest.

■ ACKNOWLEDGMENTS

We thank Elke Nadler for SEM measurements, and Marc Bröckel and Johnee Britto for first theoretical calculations. This project was funded by Deutsche Forschungsgemeinschaft (DFG) within Priority Programme “Perovskite Semiconductors: From Fundamental Properties to Devices” (SPP 2196, project no. 424708673) and SCHE1905/9-1 (project no. 426008387). We acknowledge the Max Planck Computing and Data Facility (MPCDF) for providing supercomputing resources.

■ REFERENCES

(1) Shamsi, J.; Urban, A. S.; Imran, M.; De Trizio, L.; Manna, L. Metal Halide Perovskite Nanocrystals: Synthesis, Post-Synthesis

Modifications, and Their Optical Properties. *Chem. Rev.* **2019**, *119* (5), 3296–3348.

(2) Akkerman, Q. A.; Rainò, G.; Kovalenko, M. V.; Manna, L. Genesis, Challenges and Opportunities for Colloidal Lead Halide Perovskite Nanocrystals. *Nat. Mater.* **2018**, *17* (5), 394–405.

(3) Liu, Y.; Cui, J.; Du, K.; Tian, H.; He, Z.; Zhou, Q.; Yang, Z.; Deng, Y.; Chen, D.; Zuo, X.; Ren, Y.; Wang, L.; Zhu, H.; Zhao, B.; Di, D.; Wang, J.; Friend, R. H.; Jin, Y. Efficient Blue Light-Emitting Diodes Based on Quantum-Confined Bromide Perovskite Nanostructures. *Nat. Photonics* **2019**, *13* (11), 760–764.

(4) Liu, X.-K.; Xu, W.; Bai, S.; Jin, Y.; Wang, J.; Friend, R. H.; Gao, F. Metal Halide Perovskites for Light-Emitting Diodes. *Nat. Mater.* **2021**, *20* (1), 10–21.

(5) Wu, Y.; Chen, D.; Zou, G.; Liu, H.; Zhu, Z.; Rogach, A. L.; Yip, H.-L. Strategies for Stabilizing Metal Halide Perovskite Light-Emitting Diodes: Bulk and Surface Reconstruction of Perovskite Nanocrystals. *ACS Nano* **2025**, *19* (10), 9740–9759.

(6) Kim, J. Y.; Lee, J.-W.; Jung, H. S.; Shin, H.; Park, N.-G. High-Efficiency Perovskite Solar Cells. *Chem. Rev.* **2020**, *120* (15), 7867–7918.

(7) Jena, A. K.; Kulkarni, A.; Miyasaka, T. Halide Perovskite Photovoltaics: Background, Status, and Future Prospects. *Chem. Rev.* **2019**, *119* (5), 3036–3103.

(8) Quan, L. N.; García De Arquer, F. P.; Sabatini, R. P.; Sargent, E. H. Perovskites for Light Emission. *Adv. Mater.* **2018**, *30* (45), No. 1801996.

(9) Yan, F.; Tan, S. T.; Li, X.; Demir, H. V. Light Generation in Lead Halide Perovskite Nanocrystals: LEDs, Color Converters, Lasers, and Other Applications. *Small* **2019**, *15* (47), No. 1902079.

(10) Li, M.; Liu, M.; Qi, F.; Lin, F. R.; Jen, A. K.-Y. Self-Assembled Monolayers for Interfacial Engineering in Solution-Processed Thin-Film Electronic Devices: Design, Fabrication, and Applications. *Chem. Rev.* **2024**, *124* (5), 2138–2204.

(11) Li, C.; Ganesan, P.; Li, Y.; Tang, S.; Wang, Y.; Liu, C.; Liang, L.; Yu, Y.; Yusoff, A. R. B. M.; Grätzel, M.; Gao, P. Synergistic Electron-Deficient Surface Engineering: A Key Factor in Dictating Electron Carrier Extraction for Perovskite Photovoltaics. *J. Am. Chem. Soc.* **2025**, *147* (29), 25738–25749.

(12) Yuan, L.; Xue, Q.; Wang, F.; Li, N.; Waterhouse, G. I. N.; Brabec, C. J.; Gao, F.; Yan, K. Perovskite Solar Cells and Light Emitting Diodes: Materials Chemistry, Device Physics and Relationship. *Chem. Rev.* **2025**, *125* (11), 5057–5162.

(13) Teale, S.; Degani, M.; Chen, B.; Sargent, E. H.; Grancini, G. Molecular Cation and Low-Dimensional Perovskite Surface Passivation in Perovskite Solar Cells. *Nat. Energy* **2024**, *9* (7), 779–792.

(14) Schulz, P.; Edri, E.; Kirmayer, S.; Hodes, G.; Cahen, D.; Kahn, A. Interface Energetics in Organo-Metal Halide Perovskite-Based Photovoltaic Cells. *Energy Environ. Sci.* **2014**, *7* (4), 1377.

(15) Protesescu, L.; Yakunin, S.; Bodnarchuk, M. I.; Krieg, F.; Caputo, R.; Hendon, C. H.; Yang, R. X.; Walsh, A.; Kovalenko, M. V. Nanocrystals of Cesium Lead Halide Perovskites (CsPbX_3 , X = Cl, Br, and I): Novel Optoelectronic Materials Showing Bright Emission with Wide Color Gamut. *Nano Lett.* **2015**, *15* (6), 3692–3696.

(16) Nedelcu, G.; Protesescu, L.; Yakunin, S.; Bodnarchuk, M. I.; Grotevent, M. J.; Kovalenko, M. V. Fast Anion-Exchange in Highly Luminescent Nanocrystals of Cesium Lead Halide Perovskites (CsPbX_3 , X = Cl, Br, I). *Nano Lett.* **2015**, *15* (8), S635–S640.

(17) Akkerman, Q. A.; D’Innocenzo, V.; Accornero, S.; Scarpellini, A.; Petrozza, A.; Prato, M.; Manna, L. Tuning the Optical Properties of Cesium Lead Halide Perovskite Nanocrystals by Anion Exchange Reactions. *J. Am. Chem. Soc.* **2015**, *137* (32), 10276–10281.

(18) Imran, M.; Ijaz, P.; Goldoni, L.; Maggioni, D.; Petralanda, U.; Prato, M.; Almeida, G.; Infante, I.; Manna, L. Simultaneous Cationic and Anionic Ligand Exchange For Colloidally Stable CsPbBr_3 Nanocrystals. *ACS Energy Lett.* **2019**, *4* (4), 819–824.

(19) Wahl, J.; Engelmayr, M.; Mandal, M.; Naujoks, T.; Haizmann, P.; Maier, A.; Peisert, H.; Andrienko, D.; Brütting, W.; Scheele, M. Porphyrin Functionalization of $\text{CsPbBr}_2/\text{SiO}_2$ Core–Shell Nano-

crystals Enhances the Stability and Efficiency in Electroluminescent Devices. *Adv. Opt. Mater.* **2022**, *10* (4), No. 2101945.

(20) Burrell, J. M.; Adhikari, B.; Abiodun, S. L.; Greytak, A. B. Constructing Lead Halide Perovskite Nanocrystal Surfaces. *ACS Energy Lett.* **2025**, *10* (9), 4158–4183.

(21) Alam, A.; Li, Y.; Ning, F.; Li, T.; Wang, Y. Enhancing the Optical Properties and Stability of CsPbBr₃ Quantum Dots through Ligand Modification, Encapsulation, and Interaction with a Superhydrophobic Polymer. *ACS Appl. Mater. Interfaces* **2025**, *17* (11), 17026–17035.

(22) Fiuza-Maneiro, N.; Sun, K.; López-Fernández, I.; Gómez-Graña, S.; Müller-Buschbaum, P.; Polavarapu, L. Ligand Chemistry of Inorganic Lead Halide Perovskite Nanocrystals. *ACS Energy Lett.* **2023**, *8* (2), 1152–1191.

(23) De Roo, J.; Ibáñez, M.; Geiregat, P.; Nedelcu, G.; Walravens, W.; Maes, J.; Martins, J. C.; Van Driessche, I.; Kovalenko, M. V.; Hens, Z. Highly Dynamic Ligand Binding and Light Absorption Coefficient of Cesium Lead Bromide Perovskite Nanocrystals. *ACS Nano* **2016**, *10* (2), 2071–2081.

(24) Grisorio, R.; Di Clemente, M. E.; Fanizza, E.; Allegretta, I.; Altamura, D.; Striccoli, M.; Terzano, R.; Giannini, C.; Irimia-Vladu, M.; Suranna, G. P. Exploring the Surface Chemistry of Cesium Lead Halide Perovskite Nanocrystals. *Nanoscale* **2019**, *11* (3), 986–999.

(25) Chen, Y.; Smock, S. R.; Flintgruber, A. H.; Perras, F. A.; Brutchey, R. L.; Rossini, A. J. Surface Termination of CsPbBr₃ Perovskite Quantum Dots Determined by Solid-State NMR Spectroscopy. *J. Am. Chem. Soc.* **2020**, *142* (13), 6117–6127.

(26) Kirsch, C.; Naujoks, T.; Haizmann, P.; Frech, P.; Peisert, H.; Chassé, T.; Brütting, W.; Scheele, M. Zwitterionic Carbazole Ligands Enhance the Stability and Performance of Perovskite Nanocrystals in Light-Emitting Diodes. *ACS Appl. Mater. Interfaces* **2023**, *15* (27), 32744–32752.

(27) Krieg, F.; Ochsenein, S. T.; Yakunin, S.; Ten Brinck, S.; Aellen, P.; Süess, A.; Clerc, B.; Guggisberg, D.; Nazarenko, O.; Shynkarenko, Y.; Kumar, S.; Shih, C.-J.; Infante, I.; Kovalenko, M. V. Colloidal CsPbX₃ (X = Cl, Br, I) Nanocrystals 2.0: Zwitterionic Capping Ligands for Improved Durability and Stability. *ACS Energy Lett.* **2018**, *3* (3), 641–646.

(28) Zaccaria, F.; Zhang, B.; Goldoni, L.; Imran, M.; Zito, J.; Van Beek, B.; Lauciello, S.; De Trizio, L.; Manna, L.; Infante, I. The Reactivity of CsPbBr₃ Nanocrystals toward Acid/Base Ligands. *ACS Nano* **2022**, *16* (1), 1444–1455.

(29) Dai, J.; Roshan, H.; De Franco, M.; Goldoni, L.; De Boni, F.; Xi, J.; Yuan, F.; Dong, H.; Wu, Z.; Di Stasio, F.; Manna, L. Partial Ligand Stripping from CsPbBr₃ Nanocrystals Improves Their Performance in Light-Emitting Diodes. *ACS Appl. Mater. Interfaces* **2024**, *16* (9), 11627–11636.

(30) Jayabalan, R.; Hanumantharaju, G. K.; Hettiger, T.; Sarkar, A.; Zu, F.; Ullrich, A.; Abfalterer, A.; Urban, A. S.; Koch, N.; Andrienko, D.; Scheele, M.; Brütting, W. Optimizing Carrier Balance in CsPbBr₃ Nanocrystal LEDs: The Role of Alkyl Ligands and Polar Electron Transport Layers. *Adv. Opt. Mater.* **2025**, *13* (28), No. e01361.

(31) Pan, J.; Quan, L. N.; Zhao, Y.; Peng, W.; Murali, B.; Sarmah, S. P.; Yuan, M.; Sinatra, L.; Alyami, N. M.; Liu, J.; Yassitepe, E.; Yang, Z.; Voznyy, O.; Comin, R.; Hedhili, M. N.; Mohammed, O. F.; Lu, Z. H.; Kim, D. H.; Sargent, E. H.; Bakr, O. M. Highly Efficient Perovskite-Quantum-Dot Light-Emitting Diodes by Surface Engineering. *Adv. Mater.* **2016**, *28* (39), 8718–8725.

(32) Kroupa, D. M.; Vörös, M.; Brawand, N. P.; McNichols, B. W.; Miller, E. M.; Gu, J.; Nozik, A. J.; Sellinger, A.; Galli, G.; Beard, M. C. Tuning Colloidal Quantum Dot Band Edge Positions through Solution-Phase Surface Chemistry Modification. *Nat. Commun.* **2017**, *8* (1), No. 15257.

(33) Tao, S.; Schmidt, I.; Brocks, G.; Jiang, J.; Tranca, I.; Meerholz, K.; Olthof, S. Absolute Energy Level Positions in Tin- and Lead-Based Halide Perovskites. *Nat. Commun.* **2019**, *10* (1), 2560.

(34) Lu, H.; Zhu, X.; Miller, C.; San Martin, J.; Chen, X.; Miller, E. M.; Yan, Y.; Beard, M. C. Enhanced Photoredox Activity of CsPbBr₃

Nanocrystals by Quantitative Colloidal Ligand Exchange. *J. Chem. Phys.* **2019**, *151* (20), No. 204305.

(35) Samu, G. F.; Scheidt, R. A.; Kamat, P. V.; Janáky, C. Electrochemistry and Spectroelectrochemistry of Lead Halide Perovskite Films: Materials Science Aspects and Boundary Conditions. *Chem. Mater.* **2018**, *30* (3), 561–569.

(36) Ashokan, A.; Mulvaney, P. Spectroelectrochemistry of Colloidal CdSe Quantum Dots. *Chem. Mater.* **2021**, *33* (4), 1353–1362.

(37) Min, S.; Jeon, M.; Cho, J.; Bang, J. H.; Kamat, P. V. Spectroelectrochemical Insights into the Intrinsic Nature of Lead Halide Perovskites. *Nano Converg.* **2024**, *11* (1), 49.

(38) Mulder, J. T.; Du Fossé, I.; Alimoradi Jazi, M.; Manna, L.; Houtepen, A. J. Electrochemical P-Doping of CsPbBr₃ Perovskite Nanocrystals. *ACS Energy Lett.* **2021**, *6* (7), 2519–2525.

(39) Mulder, J. T.; Monchen, J. O. V.; Vogel, Y. B.; Lin, C. T.; Drago, F.; Caselli, V. M.; Saikumar, N.; Savenije, T. J.; Houtepen, A. J. Orthogonal Electrochemical Stability of Bulk and Surface in Lead Halide Perovskite Thin Films and Nanocrystals. *J. Am. Chem. Soc.* **2024**, *146* (35), 24415–24425.

(40) Yassitepe, E.; Yang, Z.; Voznyy, O.; Kim, Y.; Walters, G.; Castañeda, J. A.; Kanjanaboos, P.; Yuan, M.; Gong, X.; Fan, F.; Pan, J.; Hoogland, S.; Comin, R.; Bakr, O. M.; Padilha, L. A.; Nogueira, A. F.; Sargent, E. H. Amine-Free Synthesis of Cesium Lead Halide Perovskite Quantum Dots for Efficient Light-Emitting Diodes. *Adv. Funct. Mater.* **2016**, *26* (47), 8757–8763.

(41) Cardona, C. M.; Li, W.; Kaifer, A. E.; Stockdale, D.; Bazan, G. C. Electrochemical Considerations for Determining Absolute Frontier Orbital Energy Levels of Conjugated Polymers for Solar Cell Applications. *Adv. Mater.* **2011**, *23* (20), 2367–2371.

(42) Schlaf, R.; Parkinson, B. A.; Lee, P. A.; Nebesny, K. W.; Jabbour, G.; Kippelen, B.; Peyghambarian, N.; Armstrong, N. R. Photoemission Spectroscopy of LiF Coated Al and Pt Electrodes. *J. Appl. Phys.* **1998**, *84* (12), 6729–6736.

(43) Wang, J.; Liu, J.; Huang, S.; Wu, X.; Shi, X.; Chen, C.; Ye, Z.; Lu, J.; Su, Y.; He, G.; Zheng, Y. High Efficiency Green Phosphorescent Organic Light-Emitting Diodes with a Low Roll-off at High Brightness. *Org. Electron.* **2013**, *14* (11), 2854–2858.

(44) Chiba, T.; Pu, Y.-J.; Miyazaki, R.; Nakayama, K.; Sasabe, H.; Kido, J. Ultra-High Efficiency by Multiple Emission from Stacked Organic Light-Emitting Devices. *Org. Electron.* **2011**, *12* (4), 710–715.